Dimensioning a recovery boiler furnace using mathematical optimization

VILJAMI MAAKALA AND PASI MIIKKULAINEN

ABSTRACT: Capacities of the largest new recovery boilers are steadily rising, and there is every reason to expect this trend to continue. However, the furnace designs for these large boilers have not been optimized and, in general, are based on semiheuristic rules and experience with smaller boilers.

We present a multiobjective optimization code suitable for diverse optimization tasks and use it to dimension a high-capacity recovery boiler furnace. The objective was to find the furnace dimensions (width, depth, and height) that optimize eight performance criteria while satisfying additional inequality constraints. The optimization procedure was carried out in a fully automatic manner by means of the code, which is based on a genetic algorithm optimization method and a radial basis function network surrogate model. The code was coupled with a recovery boiler furnace computational fluid dynamics model that was used to obtain performance information on the individual furnace designs considered.

The optimization code found numerous furnace geometries that deliver better performance than the base design, which was taken as a starting point. We propose one of these as a better design for the high-capacity recovery boiler. In particular, the proposed design reduces the number of liquor particles landing on the walls by 37%, the average carbon monoxide (CO) content at nose level by 81%, and the regions of high CO content at nose level by 78% from the values obtained with the base design. We show that optimizing the furnace design can significantly improve recovery boiler performance.

Application: Combining an optimization method with a numerical model provides an automatic tool that can be used to explore various furnace design choices to improve recovery boiler performance.

The capacities of the largest boilers being built are approximately 7000 metric tons of dry solids per day (TDS/day), and boilers as large as 12000 TDS/day have been planned. The furnace designs for these large boilers have not been optimized and usually are based on semiheuristic rules or on experience with smaller boilers. The furnace design affects boiler performance. It influences, for example, black liquor spraying, combustion air injection, volumetric heat load, char bed formation, and flow patterns within the furnace. All of these factors directly affect the combustion processes and chemical reactions taking place in the recovery boiler. Accordingly, an optimized furnace design can possibly yield significantly improved performance. If cost is included as an optimization criterion, then it too can be minimized subject to other constraints.

Recovery boiler models based on computational fluid dynamics (CFD) are valuable tools in boiler design and have been extensively used in recent years. For example, Engblom et al. [1] have used CFD modeling to study asymmetric furnace temperatures and compared the results with validation measurements. Char bed modeling and processes have been studied by Bergroth et al. [2] and Engblom et al. [3]. Vakkilainen et al. [4] have analyzed high solids black liquor firing processes using CFD and compared model predictions to measurements. Mueller et al. [5] have used CFD modeling to study the influence of liquor-to-liquor differences on the overall furnace process. Work to validate these models has been performed by Grace et al. [6].

Because it is computationally expensive to model large boilers, studying several individual design choices by using CFD modeling is challenging. The computational cost makes it infeasible to make trial-and-error comparisons between designs by running multitudinous simulations; furthermore, this method is not guaranteed to produce an improved design, let alone the best one possible. For these reasons, there is growing interest in CFD-driven optimization (CFD-optimization). The basic idea is that a CFD model is combined with an optimization method. The optimization algorithm finds the optimum by applying information about objective functions in different points of a design space, and the CFD model is used to provide this information via simulations. Surrogate models that use machine learning methods are often employed in addition, to reduce the number of CFD evaluations needed.

CFD-optimization has been used in various fields by several researchers. Thévenin and Janiga [7] present a compilation of approaches and describe how they have been used in various applications. Giannakoglou [8] provides a review that focuses on decreasing the computational cost of these methods. Saario [9] has used CFD-optimization in minimizing the

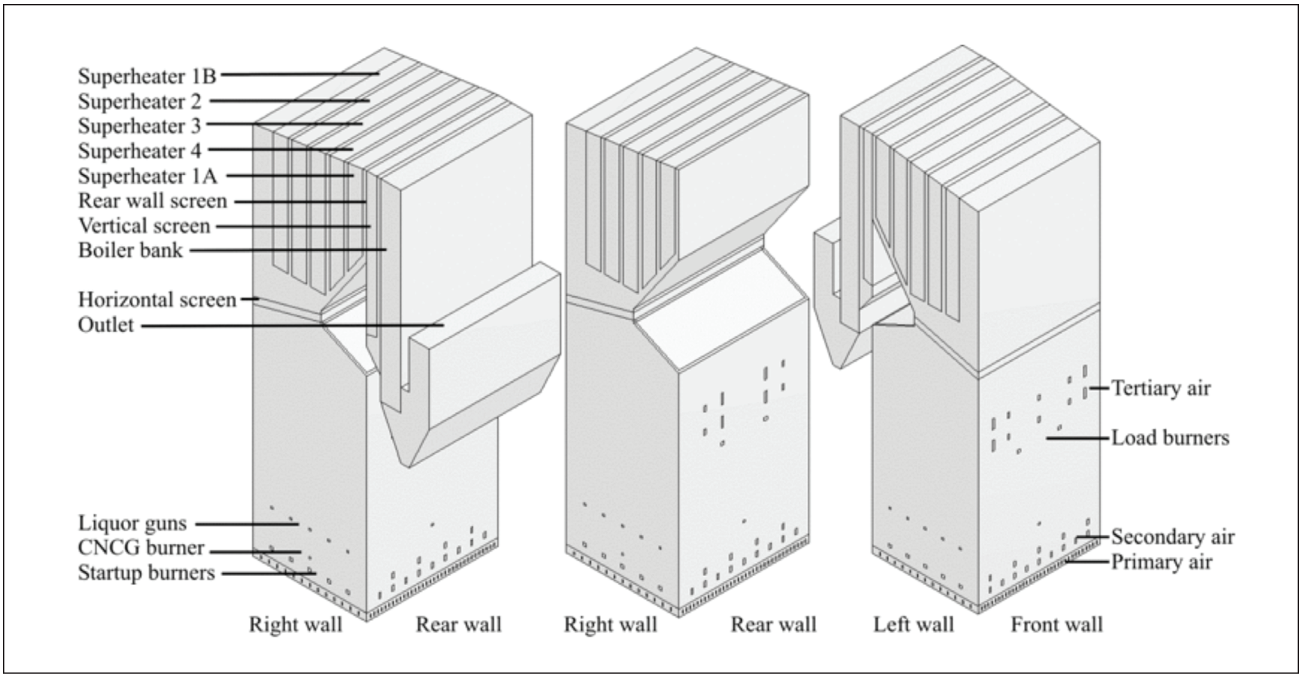

1. Recovery boiler base design showing locations of openings and heat transfer surfaces. In the middle view, the area beyond the rear wall screen is hidden so that the openings on the rear wall are visible.

NO and NH_3 emissions of a fluidized bed boiler. Foli et al. [10] have used these methods for designing a micro heat exchanger, Tahara et al. [11] in ship design, Safikhani et al. [12] to optimize cyclone separators, Mohamed et al. [13] for optimization of the airfoil shape for a Wells turbine, and Madsen et al. [14] for a diffuser shape optimization. A different approach to CFD-optimization, wherein the adjoint equations are solved, has been used in aerodynamic shape optimization by Soto et al. [15] and Fazzolari et al. [16]. However, there have been few studies, if any, in which CFD-optimization has been used in the recovery boiler sector.

This paper presents a multiobjective optimization code suitable for highly varied optimization tasks and shows its application to dimension a high-capacity (7000 TDS/day) recovery boiler furnace. The objective is to determine the furnace dimensions (width, depth, and height) that optimize eight performance criteria while satisfying additional inequality constraints. The optimization procedure is carried out in a fully automatic manner by means of the code, which is based on a genetic algorithm (GA) optimization method and a radial basis function network (RBFN) surrogate model. The code is coupled with a recovery boiler furnace CFD model that is used for obtaining performance information on the individual furnace designs under consideration.

RECOVERY BOILER DESIGNS

The designs used in this work conform to the principles for industrial design of boilers and include all features present in modern high-efficiency recovery boilers. The base design taken as a starting point in the optimization work does not correspond to any existing recovery boiler. **Figure 1** presents the base design, with the most important features specified.

The furnace width (w) in the base design is 19.4 m, the depth (d) is 16.8 m, and the height (h) is 31.5 m. Furnace height is defined in this work as the distance between the model bottom and the starting point of the nose. The furnace width, depth, and height are the design variables; these are the parameters whose values are changed in the course of the optimization work. As their values are changed, adjustments to the boiler design are performed according to the design principles programmed into the optimization code. Providing an example, **Fig. 2** shows three recovery boilers, with different furnace designs, automatically generated by the code.

The design principles determine how the complete boiler design is to be modified when the furnace dimensions are changed. The air ports and other openings are positioned on their respective walls so their relative distances from the walls and each other stay constant. The elevations of the openings from the model bottom do not change. Also, heat transfer to the superheaters, screens, and boiler bank is kept constant, and the depth of the nose is fixed at 40% of the furnace depth. Finally, the boiler geometry behind the rear wall screen is kept as similar as possible among the individual designs to minimize its impact on furnace conditions.

OPTIMIZATION PROBLEM DEFINITION

In this work, furnace geometry of a high-capacity recovery boiler is optimized according to multiple performance criteria and constraints. This multiobjective optimization problem is mathematically formulated as Eq. (1):

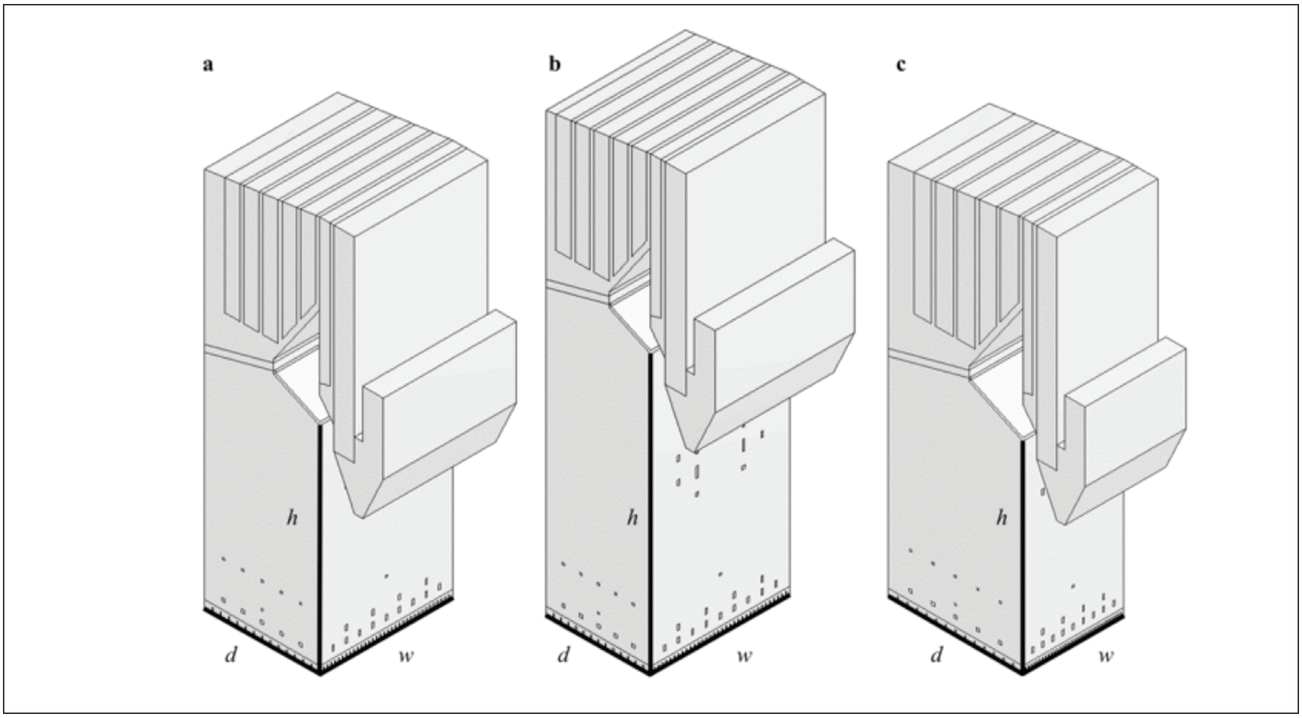

2. Boilers with different furnace designs. Also depicted are definitions of the furnace width (w), depth (d), and height (h) variables: (a) base design (w 19.4 m, d 16.8 m, and h 31.4 m); (b) wide and high furnace (w 20.0 m, d 15.0 m, and h 40.0 m); and (c) deep and low furnace (w 15.0 m, d 20.0 m, and h 30.0 m).

$$
\begin{aligned}
&\text{minimize} && f_{\mathrm{carry}}, f_{\mathrm{par}}, f_{\mathrm{CO}}, f_{\mathrm{COsp}}, f_{\mathrm{v}\sigma}, f_{\mathrm{T}\sigma}, f_{\mathrm{O2}}\\
&\text{maximize} && f_{\mathrm{low}}\\
&\text{subject to} && 988 \le g_{\mathrm{T}} \le 1008\ [^{\circ}\mathrm{C}]\\
& && g_{\mathrm{CO}} \le 200\ [\mathrm{ppmw}]\\
& && 13.0 \le w \le 27.0\ [\mathrm{m}]\\
& && \mathrm{MAX}\,(13.0, c_1(w)) \le d \le 27.0\ [\mathrm{m}]\\
& && \mathrm{MAX}\,(26.0, c_2(w,d)) \le h \le \mathrm{MIN}(45.0, c_3(w,d))\ [\mathrm{m}]
\end{aligned} \tag{1}
$$

where f_{carry}, f_{par}, f_{CO}, f_{COsp}, $f_{\mathrm{v}\sigma}$, $f_{\mathrm{T}\sigma}$, f_{O2}, and f_{low} are objective functions; g_{T} and g_{CO} are constraint functions; and w, d, and h are the furnace width, depth and height variables, in that order. MAX and MIN are functions that return the largest and smallest of their arguments, respectively. The functions $c_1(w)$, $c_2(w,d)$, and $c_3(w,d)$ constrain the furnace dimensions in accordance with boiler design principles. The units of the constraints are given in brackets after the equations. Design points $\vec{x} = (w,d,h)$ respecting the bounds for the w, d, and h variables constitute the design space, D. The points in this space that also satisfy the constraints for g_{T} and g_{CO} form the feasible space, S. **Table I** summarizes the meanings, optimization targets, chosen importance values, and chosen weights of the variables, objective functions, and constraint functions.

The boundaries for the design variables in Eq. (1) are set in line with established recovery boiler design practices. Furnace w and d are constrained to between 13 m and 27 m and h to between 26 m and 45 m. These constraints exclude unreasonably high and low w, d, and h height values from the design space. Furthermore, the furnace depth is constrained from below by the function $c_1(w)$, which gives a minimum depth for a boiler of a given width that can accommodate the superheaters. The furnace height is further constrained by two functions: $c_2(w,d)$ and $c_3(w,d)$. These ensure that the residence time of the gas between upper tertiary air and nose level is within reasonable limits.

The mean carbon monoxide (CO) content and temperature at the nose level are constrained by the inequality constraints on the g_{CO} and g_{T} functions. The g_{CO} is constrained to below 200 ppmw, because boiler designs with high CO content at nose level are not interesting in practice. Mean nose temperature g_{T} is constrained to between 988ºC and 1008ºC because the heat balance calculated for the design, which also imposes boundary conditions in the computational model, is based on a nose temperature of 998ºC.

The f_{carry}, f_{CO}, f_{low}, and f_{O2} objective functions assess the quality and completeness of the combustion processes in the furnace. The f_{low} objective is included and maximized because a high average temperature in the lower furnace area is an indication that most of the combustion is occurring there. Noncombusted material above nose level fouls the heat transfer surfaces and causes emissions. These four objectives are often conflicting and it is important to optimize them together. The f_{par} objective refers to the number of liquor particles landing on the walls. It is minimized because a large amount

Function	Meaning	Target	Importance	Weight
w	Furnace width (m)	Satisfy constraints	Essential	--
d	Furnace depth (m)	Satisfy constraints	Essential	--
h	Furnace height (m)	Satisfy constraints	Essential	--
g_{CO}	CO content at nose level (ppmw)	Satisfy constraints	Essential	--
g_T	Temperature at nose level (°C)	Satisfy constraints	Essential	--
f_{carry}	Carryover at nose level (kg/s)	Minimize	1	0.30
f_{par}	BL landing on walls (% wet flow)	Minimize	1	0.30
f_{CO}	CO content at nose level (ppmw)	Minimize	2	0.10
f_{low}	Lower furnace temperature (°C)	Maximize	2	0.10
f_{COsp}	CO spikes at nose level (% area)	Minimize	3	0.05
$f_{v\sigma}$	y-velocity σ at nose level (m/s)	Minimize	3	0.05
$f_{T\sigma}$	Temperature σ at nose level (°C)	Minimize	3	0.05
f_{O2}	O_2 content at nose level (wt%)	Minimize	3	0.05

I. Meanings, optimization targets, chosen importance values, and chosen weights of the variables, objective functions, and constraint functions. (CO = carbon monoxide, BL = black liquor, y-velocity = upward velocity, σ = standard deviation, 1 = highest importance value, and 3 = lowest importance value).

of black liquor sprayed on the walls can lead to asymmetrical or unsteady boiler operation. When we set this objective, we assumed that minimizing the amount of black liquor landing on the walls would lead to an increase in the amount landing on the char bed and the amount of in-flight combustion would not change considerably. We assumed this because only the furnace dimensions are modified. The f_{COsp}, $f_{v\sigma}$, and $f_{T\sigma}$ objectives are indicators of balance in boiler operation and the associated values reflect the evenness of the profiles at nose level. The value of f_{COsp} is the relative area in which the CO content is higher than 300% of the mean value at the level in question. These areas of high CO content often account for most of the total CO emitted and can result from imbalances in boiler operation.

Preferences pertaining to the relative importance of the individual objectives are taken into account in the optimization because not all criteria for a good boiler design are equally important. Preference-based guidance is implemented into the code of the GA optimization method through a weighting scheme proposed by Cvetković and Parmee [17]. Weighted dominance, which is inspected in the scheme when two feasible solutions are being compared, is defined for a minimization problem as Eq. (2):

$$\vec{x}_i \text{ dominates } \vec{x}_j \Leftrightarrow \sum_{k: f_k(\vec{x}_i) \leq f_k(\vec{x}_j)} w_k \geq \tau \tag{2}$$

where $\vec{x}_i$ and $\vec{x}_j$ are two solutions, $f_k(\vec{x})$ are the objective functions, w_k are the weights associated with each $f_k(\vec{x})$, and τ is a parameter for the minimum level of dominance. Table I shows the weights used, which are based on the importance values selected for the objectives. The minimum level of dominance $\tau = 0.85$ is used.

CFD-OPTIMIZATION METHOD

The CFD-optimization code integrates a recovery boiler CFD model with an optimization algorithm, a surrogate model, and a CFD preprocessing code. **Figure 3** presents an outline of the CFD-optimization method used. Similar frameworks have been presented before by Thévenin and Janiga [7] and Giannakoglou [8], for example. The optimization algorithm applied is a binary-coded elitist nondominated sorting genetic algorithm (NSGA-II), introduced by Deb et al. [18]. The surrogate model is based on locally trained RBFN, which have been researched in the context of optimization by Giannakoglou [8] and studied further by Duvigneau and Visonneau [19].

The optimization algorithm begins with an initial population of random design points. The algorithm uses information from the CFD and surrogate models to evolve the population toward the Pareto front, which is defined as the group of optimal solutions to the given optimization problem. On the Pareto front, none of the objective functions can be improved any more without worsening at least one of the others. At the beginning of each generation, the optimization algorithm asks the surrogate model to evaluate the population of design points. The best point is first sent to the preprocessor, then

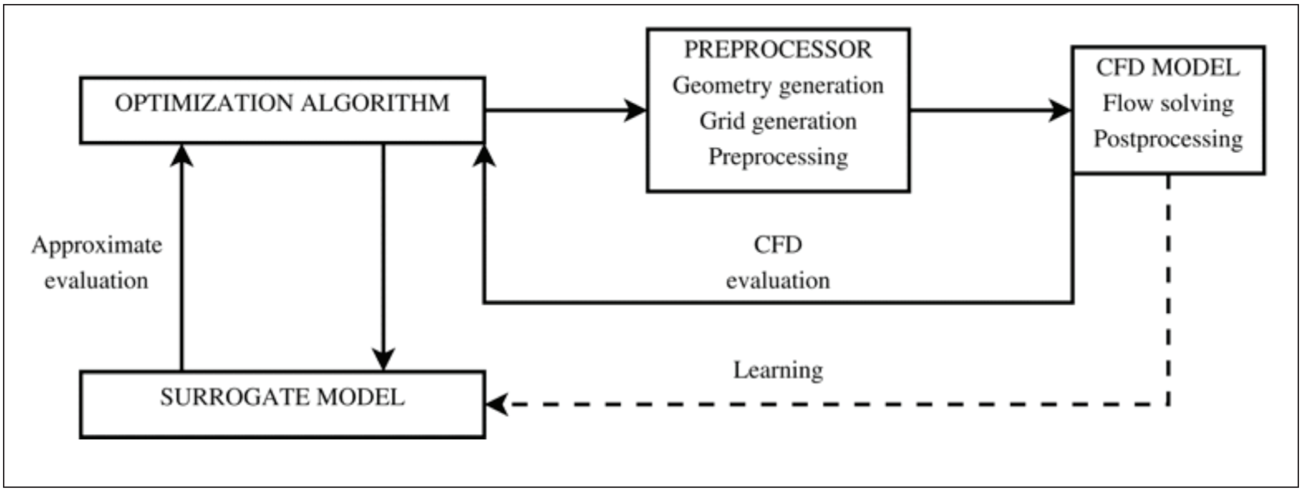

3. Outline of the CFD-optimization code. The boxes represent subroutines and the arrows indicate directions of information flow. Some functions of the subroutines are listed below their titles.

to the CFD model. The CFD model solves for the objective and constraint function values at the design point; these values are used to update the model's evaluation and the database of the surrogate model. After this, the optimization algorithm constructs an improved population of design points and advances to a new generation.

The surrogate model is used for fast approximate evaluations and for gathering information acquired via CFD to reduce future work. It is initialized with a training database before the optimization and then learns from each CFD evaluation during the run. In this work, the training database was built through evaluation of 63 quasirandom points in design space *D* through a procedure that ensured its global coverage. The training database size was limited by the 6 weeks of computing time available for training.

Table II shows the values of the parameters used in the algorithms. The NSGA-II parameters are set to similar values as in Deb et al. [18] and the RBFN parameters according to the recommendations of Duvigneau and Visonneau [19]. The number of generations run and the training database size became known after running the code.

The preprocessor builds a recovery boiler geometry for a given design point in accordance with the design rules. It builds a computational grid for this geometry with an automated method using ANSYS DesignModeler and Meshing programs (ANSYS Inc.; Canonsburg, PA, USA). The method makes predominantly hexahedral meshes (more than 95% hexahedral cells), with tetrahedral cells in areas where hexahedral cells are hard to place. Local mesh refinements are handled via hanging node adaptation. The grids have between 0.5 million and 1 million cells, approximately, and the total cell counts are limited by the computational resources available. **Figure 4** shows two views of the grid for the boiler base design, which is taken as a starting point in the optimization process. After building the grid, the preprocessor assigns simulation settings and boundary conditions for the case. To speed up convergence, fields of the variables to be solved are initialized with simulation results for the closest design point in *D* by Euclidean distance. Finally, the preprocessor sends the case to the CFD model.

Parameter	Symbol	Value
NSGA-II		
Population size	n_{ind}	200
Generations	--	40
Design variable string length	b	10
Crossover probability	p_c	1.0
Mutation probability	p_m	$1.0/(bn_{dv})$
Minimum level dominance	τ	0.85
RBFN		
Training database size	–	63
Attenuation coefficient	e	100
Local database size	d	10

II. Parameters used in the optimization (NSGA-II) and surrogate model (RBFN) algorithms. $n_{dv} = 3$ ***refers to the number of design variables.***

The CFD model is based on ANSYS Fluent 14.0 customized with numerous in-house submodels. The CFD model has been used in several recovery boiler furnace combustion studies, and validation work of its performance has been carried out by Miikkulainen, Pakarinen, and Metsämuuronen [20] and Saviharju and others [21-23].

In the model, equations are solved in a steady state and the segregated SIMPLE scheme [24] is used to resolve the pressure-velocity coupling. Turbulence is modeled with the standard k-ε model [25], and the P-1 radiation heat transfer model [26] is used. Gas phase species transport equations for H_2O, O_2, CO, CO_2, H_2, CH_4, H_2S, SO_2, Na, NaCl, NaOH, and Na_2SO_4 are solved. The mass fraction of N_2 is solved for by means of the mass fractions of the other species. Chemical reaction rates are determined through the finite-rate/eddy-dissipation

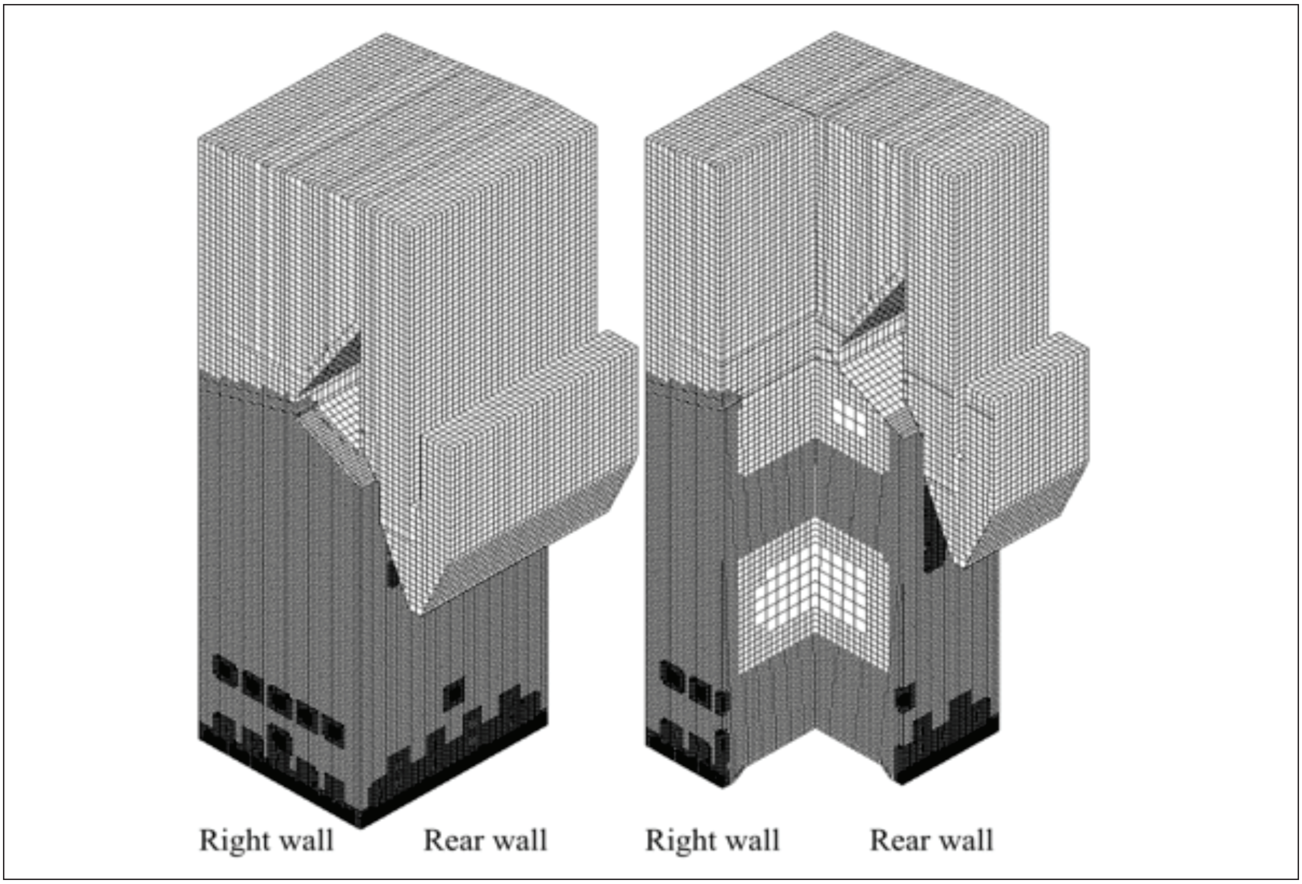

4. Two views of the computational grid for the recovery boiler base design. Grid refinements can be seen near the openings, air port levels, and furnace walls. In the right view, one corner of the grid is cut off to render the grid inside the furnace visible

model [27]. Black liquor particle trajectories and reactions are modeled with an in-house code based on the ANSYS Fluent 14.0 discrete phase model [28]. The in-house code is derived from the work of Kankkunen and Miikkulainen [29], Miikkulainen et al. [30], and Kankkunen et al. [31]. The heat transfer surfaces are modeled as momentum and heat sinks in the volumes they occupy. Char bed shape is fixed. Local conditions affect the amount of char combusted in the various areas of the bed, but scaling is used to ensure that all of the char is combusted.

RESULTS

We solved the furnace geometry optimization problem using the presented CFD-optimization code on a computer with four AMD Opteron 6176 SE processors (Advanced Micro Devices; Suwanee, GA, USA) having 12 cores each and 64 GB of RAM. The CFD simulations were solved in parallel, with all 48 cores available. Convergence was monitored both by visual inspection of the movement of the design points in the design space and by the average fitness value of the population as a function of generations. In this work, the fitness value of a design was defined as one for the nondominated designs in the population, according to Eq. (2). A fitness value of 2 was given to all the nondominated designs in the rest of the population after removing the designs with a fitness value of one. This process was continued until all of the designs were ranked.

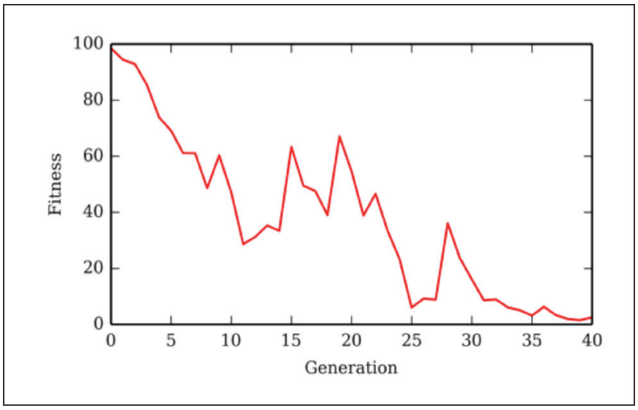

5. Average fitness value of the population as a function of generations.

Figure 5 shows the average fitness value of the population as a function of generations. The fitness value has a decreasing trend as the generations advance, but sometimes it increases sharply and then decreases again. The increases are normal because the algorithm continuously searches new regions of the design space for better solutions. The figure

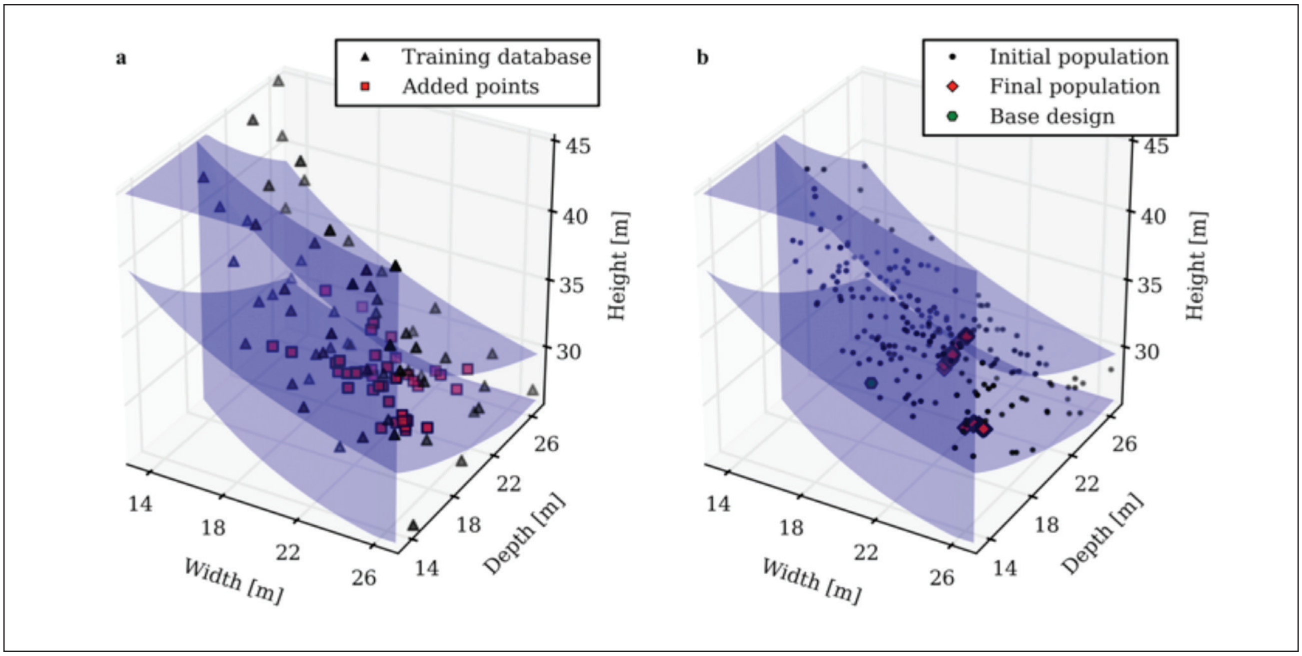

6. (a) Training database (63 points) and points added to the database during CFD-optimization (40 points). (b) Initial and final populations (200 points each) alongside the base design. The design space is constrained within the surfaces indicated in blue.

shows that the population converges to an average fitness value of 1 at around 40 generations. At this point, the population was also no longer moving in the design space; therefore, the optimization appeared converged by both metrics and we stopped the optimization code. In addition, we had reached the 4-week limit on the computing time we had available for the optimization run. Strictly speaking, it is still possible for the solutions to improve even though the average fitness value is already 1; in practice, however, it signals that the algorithm is converging.

Figure 6a shows the training database (63 points) and the points added to the database during the CFD-optimization (40 points). Some points in the training database are outside the constraining surfaces because they were solved before the exact constraint functions were known. These points can be used in approximate evaluations near the boundaries.

Figure 6b shows the initial and final populations (200 points each), along with the base design. The final population is the Pareto front obtained, which consists of the optimal solutions found to Eq. (1). The designs on the Pareto front have low furnace heights, from 28.8 m to 30.5 m, and have large furnace floors when compared to the base design. The furnace widths range from 20.0 m to 24.9 m and the depths from 16.7 m to 24.7 m. The Pareto front features solutions both with width exceeding depth and with width less than depth. The solutions exhibit clustering in design space D, and the Pareto front is discontinuous. We suspect that the code incorrectly predicts some regions of D to be infeasible because of iteration errors in the values obtained for g_{CO}, the CO content at nose level. Most likely, the final population does not represent the actual Pareto front completely. Constraining the g_{CO} value to below 200 ppmw was not a good choice, because practice has shown that it is challenging to find an accurate steady-state solution for CO content using recovery boiler furnace CFD models. In converged simulations, it is often observed that CO content at nose level still fluctuates considerably as a function of the number of iterations. This problem could have been alleviated by employment of more smoothing in the RBFN surrogate model to inhibit overfitting to the errors in the evaluations.

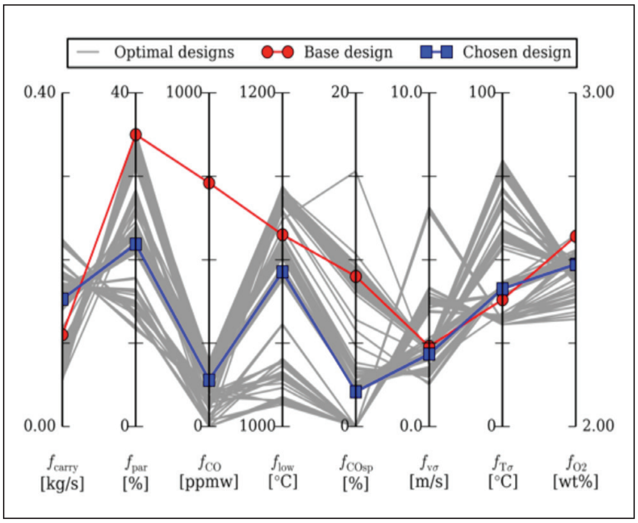

7. Objective function values for the optimal designs (Pareto front); base design, which was used as a starting point; and chosen design. Each polyline corresponds to a different design point.

Figure 7 presents the objective function values for the optimal solutions, (i.e., the Pareto front) in a parallel coordinate representation. The optimal solutions show objective

Variable or Parameter	Range on Pareto Front	Chosen Design	Base Design
Furnace width (*w*) (m)	20.0-24.9	20.1	19.4
Furnace depth (*d*) (m)	16.7-24.7	23.3	16.8
Furnace height (*h*) (m)	28.8-30.5	29.3	31.4
Floor area (m^2)	408-497	468	326
Furnace volume (m^3)	12400-14800	13700	10200
Hearth solids loading (HSL) (kgds/sm^2)	0.16-0.20	0.17	0.25
Hearth heat release rate (HHRR) (kW/m^2)	2300-2800	2400	3500
Volumetric heat input (VHI) (kW/m^3)	76-90	82	110

III. Ranges of values that the solutions on the Pareto front produce for some common furnace sizing parameters.

function values that are, in general, good in terms of recovery boiler performance and within believable bounds. Compared to the base design, all of the optimal designs are better because they satisfy the $g_{CO} \leq 200$ ppmw constraint. The base design is not especially good with respect to any of the objectives, and it has a particularly high value for the number of particles landing on the walls.

We chose one solution from the Pareto front and propose it as a better furnace design because it has good overall performance in the objectives and provides clear improvements over the base design. The number of particles landing on the walls is reduced from 35% to 22% of wet flow (37% improvement), the CO content at nose level from 730 ppmw to 140 ppmw (81% improvement), and the number of CO spikes from 9% to 2% of the area at nose level (78% improvement). The chosen design and base design display roughly equal performance for the other objectives. The chosen design has a 20.1-m furnace width, 23.3-m depth, and 29.3-m height. When compared to the base design, which has a 19.4-m furnace width, 16.8-m depth, and 31.4-m height, the chosen design has a considerably deeper furnace and a larger floor area. The furnace height in the chosen design is lower than the corresponding value in the base design.

Table III presents the ranges of values that the solutions on the Pareto front produce for some common furnace sizing parameters. The table also shows these values specifically for the chosen and the base design. Parameter values have been calculated according to Vakkilainen [32]. The most important parameters are hearth heat release rate (HHRR) and volumetric heat input (VHI), which refer to the heat load of the furnace floor and the heat load of the total furnace volume, respectively. The hearth solids loading (HSL) value indicates the furnace floor black liquor dry solids load and is analogous to the HHRR in this case, because the liquor composition remains constant.

The optimal solutions show significantly lower values than the base design for the HSL, HHRR, and VHI parameters. Vakkilainen [32] writes that typical HHRR values range from 2700 kW/m^2 to 3300 kW/m^2 in modern recovery boilers. Relative to these values, the base design shows heavy loading and the optimal designs have modest loads. Even though the optimal designs have lower furnace heights than the base design, the furnace volumes are higher and VHIs lower than in the base design. In this optimization case, better boiler operation with respect to combustion is achieved with lower HHRR and VHI values than in the base design. Even though

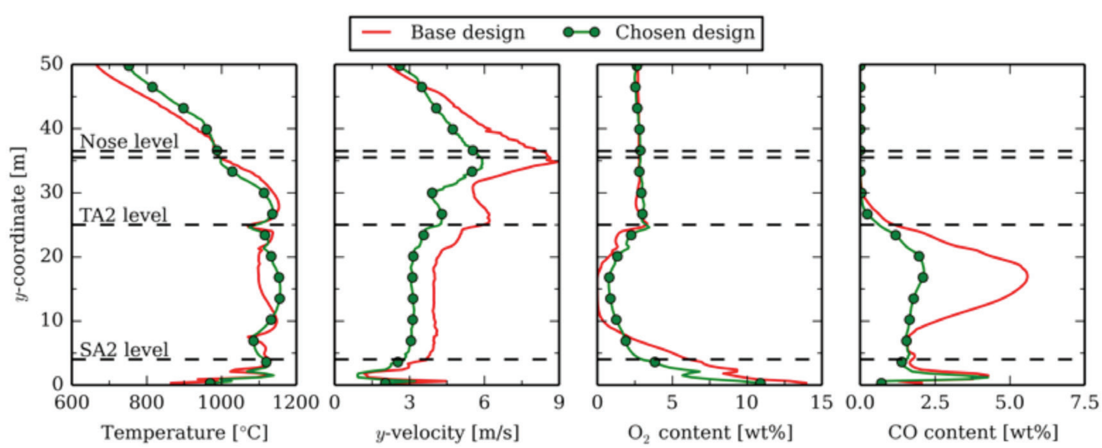

8. Mean profiles of various quantities as functions of y-coordinate in base and chosen design. The base design has its nose level at 36.5 m and the chosen design has its nose level at 35.5 m. SA2 refers to the upper secondary air level and TA2 refers to the upper tertiary air level.

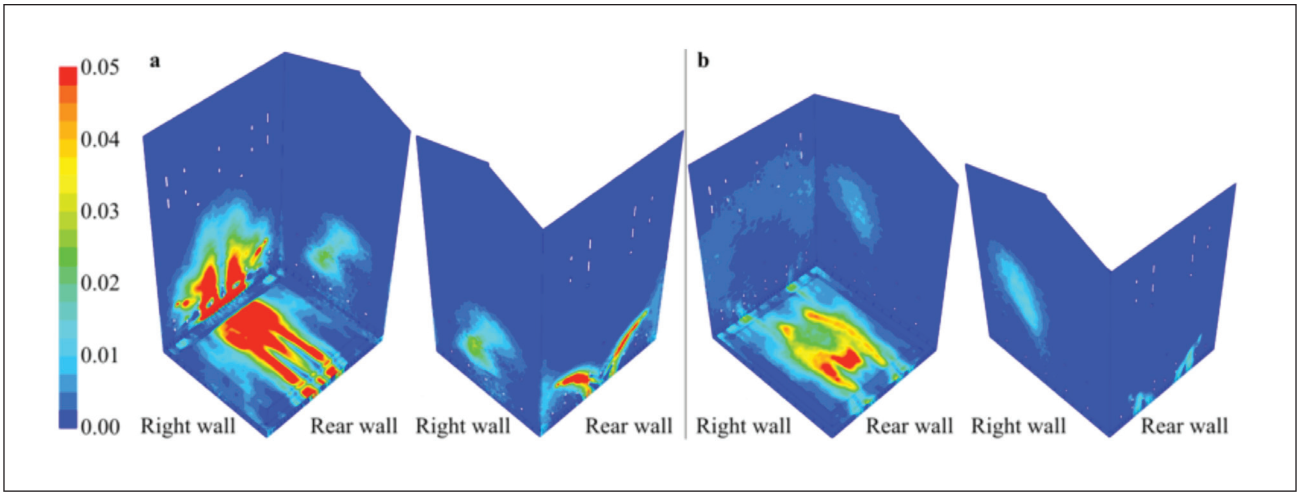

9. Carbon landing rate contours (in kg/m²s) for char bed and furnace walls: (a) base design and (b) chosen design.

the optimal designs are better from a combustion standpoint, it is not clear which design is the most cost-effective in practice. Future work should take cost into account in the definition of the optimization problem.

Figure 8 presents mean profiles of temperature, upward velocity (y-velocity), CO content, and O_2 content as functions of the upward coordinate (y-coordinate) in the base and chosen design. Above nose level, the temperature profiles show some differences because, even though the rate of heat transfer to each superheater is the same between the two designs, the absolute locations of the superheaters differ. The temperature of the gas after the heat transfer surfaces should be the same between these designs because they have the same overall heat balance. Below nose level, the temperature profiles are similar because nose temperature g_T is constrained in Eq. (1). The rate of heat transfer to the furnace walls in all of the optimal designs, including the chosen design, is the same as in the base design. Consequently, the average heat flux to the furnace walls and the total wall areas are roughly the same.

In Fig. 8, the y-velocities along the height of the boiler are lower in the chosen design than in the base design. This is understandable because the chosen design has a larger floor area and the same amount of air and liquor is injected into the boiler. The higher y-velocity profile can partly explain the large number of liquor particles landing on the walls in the base design. In the chosen design, a lower upward velocity profile increases the residence time of the gas in the furnace, so combustion has more time to complete. There is also less O_2 in the lower furnace area in the chosen design than in the base design, which may mean that more combustion is taking place there. In the base design, the CO content shows high values between the liquor gun level (7.6 m) and the upper tertiary air level; this is caused by the large amount of liquor landing on the walls. When carbon is released from the liquor particles in a low-O_2 environment, CO is formed and combusts at the tertiary air level, which is less desirable than combustion in the lower furnace.

Figure 9 shows patterns for carbon landing rate in the furnace floor and wall areas in the base and chosen designs. In the base design, the rate of carbon landing on the char bed is high near the middle along the width and more carbon lands near the front wall than near the rear wall. Uniform carbon landing over the entire furnace floor would be desirable. The total amount of black liquor landing on the bed is low (18% of wet flow). A large amount of liquor lands on the furnace walls (35% of wet flow), especially the front wall (22% of wet flow). Also, the side wall liquor guns closest to the walls spray a large amount of liquor on the front and rear walls. The carbon landing rate pattern for the char bed is much more even in the chosen design than in the base design, the spread is better over width and depth, and the regions of very high carbon landing rate are smaller. The total amount of black liquor landing on the bed (30% of wet flow) is significantly higher than in the base design and the amount landing on the walls is smaller (22% of wet flow). In the chosen design, the side wall guns are further from the front and rear walls because the furnace has greater depth (23.3 m) than the base design (16.8 m). For this reason, the amount of liquor sprayed by these guns onto the front and rear wall is reduced.

CONCLUSION

The CFD-optimization code found a Pareto front of optimal furnace designs for the high-capacity (7000 TDS/day) recovery boiler. Compared to the base design, which was used as a starting point, the optimal solutions have large furnace floors, low furnace heights, and low volumetric heat loads. The complete Pareto front was not found because the code incorrectly predicted some regions of the design space to be infeasible. This problem was caused by iteration errors in the values obtained for the CO content at nose level and could have been partially prevented through use of more smoothing in the surrogate model. We propose one solution from the Pareto front as a better furnace design because it has good overall performance and it provides clear improvements over the base design. The number of particles landing on the walls is reduced from 35% to 22% of wet flow (37% improvement), the CO content at nose level is reduced from 730 ppmw to 140 ppmw (81% improvement), and the number of CO spikes is reduced from 9% to 2% of the area at nose level (78% improvement).

The designs on the Pareto front obtained in this work are optimal from a combustion perspective but are expensive in practice. By taking cost factors into account in the optimization problem definition, it is possible to find optimal designs that are also cost-effective.

Our future work will investigate possibilities for use of the CFD-optimization code in different applications. We will develop the code by improving the smoothing properties of the surrogate model and by incorporating a more intuitive method of introducing designer preferences in the optimization algorithm. Furthermore, we will consider including local optimization methods into the code to improve its convergence speed and accuracy near the Pareto front. **TJ**

ACKNOWLEDGMENTS

This paper is based in part on the Master's thesis of Viljami Maakala, "Multi-objective optimization of recovery boiler dimensions using computational fluid dynamics." The authors thank Professor Timo Siikonen of Aalto University and all others who contributed to that work.

LITERATURE CITED

1. Engblom, M., Miikkulainen, P., Brink, A., et al., *TAPPI J.* 11(11): 19(2012).
2. Bergroth, N., Engblom, M., Mueller, C., et al., *TAPPI J.* 9(2): 6(2010).
3. Engblom, M., Bergroth, N., Mueller, C., et al., *TAPPI J.* 9(2): 15(2010).
4. Vakkilainen, E., Kjäldman, L., Taivassalo, V., et al., *Int. Chem. Recovery Conf.*, TAPPI PRESS, Atlanta, GA, USA, 1998, p. 245.
5. Mueller, C., Eklund, K., Forssen, M., et al., *Int. Chem. Recovery Conf.*, TAPPI PRESS, Atlanta, 2004, p. 979
6. Grace, T.M., Lien, S., Schmidl, W., et al., *Int. Chem. Recovery Conf.*, TAPPI PRESS, Atlanta, 1998, p. 271.
7. Thévenin, D. and Janiga, G. (Eds.), *Optimization and Computational Fluid Dynamics*, Springer, Berlin, 2008.
8. Giannakoglou, K.C., *Prog. Aerosp. Sci.* 38(1): 43(2002).
9. Saario, A., "Mathematical modeling and multiobjective optimization in development of low-emission industrial boilers," Ph.D. thesis, Tampere University of Technology, Tampere, Finland, 2008.
10. Foli, K., Okabe, T., Olhofer, M., et al., *Int. J. Heat Mass Transfer* 49(5): 1090(2006).
11. Tahara, Y., Tohyama, S., and Katsui, T., *Int. J. Numer. Methods Fluids* 52(5): 499(2006).
12. Safikhani, H., Hajiloo, A., and Ranjbar, M.A., *Comput. Chem. Eng.* 35(6): 1064(2011).
13. Mohamed, M.H., Janiga, G., Pap, E., et al., *Energy* 36(1): 438(2011).

ABOUT THE AUTHORS

We researched combining optimization methods with numerical models so that existing models can be better used when searching for improved designs. We feel that by using optimization, many existing designs can be improved and new, optimal ones can be designed right from the start.

Optimization combined with computational fluid dynamics (CFD) has been previously studied, but mainly in applications of relatively low computational cost. We applied the methodology to recovery boilers and showed how it can be used for this application, wherein CFD evaluations are challenging and can be computationally very expensive.

The high computational cost of the CFD evaluations and the numerical uncertainty involved with them posed the greatest challenges. To make the optimization possible despite the high computational cost, we used a surrogate model to reduce the amount of CFD evaluations needed. The surrogate model can also partially smooth out the numerical uncertainty when it has enough information available. This did not work as well as we hoped in this work and will be improved in the future.

When we optimized the recovery boiler furnace design, it was surprising to see how greatly it affected the performance of the whole boiler. Modifying the furnace design clearly affected the combustion processes and chemical reactions taking place in the recovery boiler. We saw that an optimized furnace design can yield significantly improved recovery boiler performance.

Optimization can be used to find designs or operation modes that yield improved performance within designer-defined constraints. If cost is included as an optimization criterion, then cost too can be minimized subject to other constraints.

Our future work will involve using the developed CFD-optimization code in different applications. We will develop the surrogate model so that it better takes into account the numerical uncertainties in the CFD solutions. We will also implement local optimization methods into the code to improve its convergence speed and accuracy.

Maakala

Miikkulainen

Maakala is development engineer and Miikkulainen is sales manager, Andritz Oy, Helsinki, Finland. Email Maakala at viljami.maakala@andritz.com.

14. Madsen, J.I., Shyy, W., and Haftka, R.T., *AIAA J.* 38(9): 1512(2000).
15. Soto, O., Löhner, R., Yang, C., *Int. J. Numer. Methods Heat Fluid Flow* 14(6): 734(2004).
16. Fazzolari, A., Gauger, N.R., and Brezillon, J., *J. Comput. Appl. Math.* 203(2): 548(2007).
17. Cvetković, D. and Parmee, I.C., *IEEE Trans. Evolu. Comput.* 6(1): 42(2002).
18. Deb, K., Pratap, A., Agarwal, S., et al., *IEEE Trans. Evolu. Comput.* 6(2): 182(2002).
19. Duvigneau, R. and Visonneau, M., *Int. J. Numer. Methods Fluids* 44(11): 1257(2004).
20. Miikkulainen, P., Pakarinen, L., and Metsämuuronen, N., *Int. Chem. Recovery Conf.*, TAPPI PRESS, Atlanta, 2010, p. 60.
21. Saviharju, K., Pakarinen, L., Wag, K., et al., *Int. Chem. Recovery Conf.*, TAPPI PRESS, Atlanta, 2004, p. 247.
22. Saviharju, K., Pakarinen, L., Kyttälä, J., et al., “Modelling and feedback measurements give new understanding about recovery boiler behavior,” *7th Int. Colloq. Black Liquor Combust. Gasif.*, Jyväskylä, Finland, Available [Online] http://www.eng.utah.edu/~whitty/blackliquor/colloquium2006/presentations/3.1%20-%20Saviharju%20-%20Modelling%20and%20Feedback%20for%20RB.pdf <25Feb2015>.
23. Saviharju, K., Pakarinen, L., Kyttälä, J., et al., *Int. Chem. Recovery Conf.*, TAPPI PRESS, Atlanta, 2007, p. 469.
24. Patankar, S.V. and Spalding, D.B., *Int. J. Heat Mass Transfer* 15(10): 1787(1972).
25. Launder, B.E. and Sharma, B.I., *Lett. Heat and Mass Transfer* 1(2): 131(1974).
26. ANSYS Inc., “P-1 radiation model theory,” in *Fluent 14.0 Theory Guide*, Canonsburg, PA, USA, 2011.
27. ANSYS Inc., “The generalized finite-rate formulation for reaction modeling,” in *Fluent 14.0 Theory Guide*, Canonsburg, PA, 2011.
28. ANSYS Inc., “Discrete phase,” in *Fluent 14.0 Theory Guide*, Canonsburg, PA, 2011.
29. Kankkunen, A. and Miikkulainen, P., “Particle size disribution of black liquor sprays with a high-solids content in recovery boilers,” *IFRF Combustion J. [online]* Article No. 200308, December 2003.
30. Miikkulainen, P. and Kankkunen, A., Järvinen, M., et al., *TAPPI J.* 8(1): 36(2009).
31. Kankkunen, A., Miikkulainen, P., Järvinen, M., *TAPPI PEERS Conf.*, TAPPI PRESS, Atlanta, 2011, p. 434.
32. Vakkilainen, E., *Kraft Recovery Boilers—Principles and Practice*, Suomen Soodakattilayhdistys, Helsinki, 2005.